Journal of Thermal Engineering, Vol. 6, No. 4, pp. 521-543, July, 2020
Yildiz Technical University Press, Istanbul, Turkey

# MAGNETIC FIELD EFFECT ON THE HEAT TRANSFER IN A NANOFLUID FILLED LID DRIVEN CAVITY WITH JOULE HEATING

Mohammad Ali Taghikhani[1,*]

## ABSTRACT

In this paper, the effects of magnetic field, Joule heating and volumetric heat generation on the heat transfer and fluid flow in a Cu-Water nanofluid filled lid driven cavity using enhanced streamfunction–velocity method are investigated. The cavity is heated by a uniform volumetric heat density and side walls have constant temperature. The top wall moves with constant velocity in +x direction, while no-slip boundary conditions are imposed on the other walls of the cavity. An inclined fixed magnetic field is applied to the left side wall of the cavity. The dimensionless governing equations are solved numerically for the stream function and temperature using finite difference method for various Richardson($Ri$), Reynolds($Re$), Hartmann ($Ha$), Eckert($Ec$)numbers, magnetic field angle($\alpha$) and solid volume fraction of the nanofluid($\phi$) in MATLAB software. To discretize the streamfunction-velocity formulation, a five point constant coefficient second-order compact finite difference approximation which avoids difficulties inherent in the conventional streamfunction–vorticity and primitive variable formulations is used. The stream function equation is solved using fast Poisson's equation solver on a rectangular grid (POICALC function in MATLAB) and the temperature equation is solved using Jacobi bi-conjugate gradient stabilized (BiCGSTAB) method. The heat transfer within the cavity is characterized by Nusselt number ($Nu_1$). The results show that $Nu_1$ is significantly increased by increasing $Ri$ and $\phi$ and increasing the Reynolds number enhances convective cooling. The heat transfer within the cavity is decreased by increasing Hartmann number which improves conduction heat transfer and reduces $Nu_1$. Joule heating has a negative effect on the convection within the cavity and convection is decreased by increasing the value of $Ec$. It can be investigated that $Nu_1$ is decreased by increasing $Ec$ due to the strong distortion effect of Joule heating on convection current of heat transfer.

***Keywords:*** *Magnetic Field, Nano-fluid, Lid Driven Cavity, Stream Function-Velocity, Joule Heating, Volumetric Heat Generation*

## INTRODUCTION

Magnetic field effects on the heat transfer and fluid flow in fluids and nanofluids have important applications in many engineering areas and have been investigated by a number of researchers. In industrial problems, flow of an electrically conducting fluid, subjected to a magnetic field, is used, thus the fluid experiences a Lorentz force, and its effect is to reduce the flow velocities which affect the heat transfer rate. The study in [1] shows that the magnetic field suppresses the natural-convection currents and the magnetic field strength is one of the most important factors for crystal formation. The transient convective motion and heat transfer in a square cavity are investigated in [2] where the horizontal walls are adiabatic and the vertical walls are maintained at different constant temperatures. An analytical solution to the magneto-hydrodynamic (MHD) flow equations is proposed in [3] and the effect of a transverse magnetic field on buoyancy driven convection is modeled. The natural convection within rectangular cavity with a transverse magnetic field is studied numerically in [4] where one vertical wall is cooled and the other one heated while the top and bottom walls are insulated. The transient MHD equations are solved using the control volume algorithm in [5-7]. The solutions of the two-dimensional steady state magneto-hydrodynamic flows are proposed in [8-13], using finite difference and finite element methods (FDM and FEM). Steady state laminar natural convection MHD flow equations in a rectangular enclosure are solved numerically for the stream function, vorticity and temperature in [14-17].

Magnetic field effect on mixed convection heat transfer of nanofluids flow in a wavy channel is studied using mixture model and so, the effects of nano-particle volume fraction, sine wave amplitude, Reynolds number, Grashof

*This paper was recommended for publication in revised form by Regional Editor Alibakhsh Kasaeian*
*[1]Department of Engineering, Imam Khomeini International University, Qazvin, Iran*
**E-mail address: taghikhani@eng.ikiu.ac.ir*
*Orcid id: 0000-0002-9528-096X*
*Manuscript Received 21 April 2018, Accepted 25 June 2018*

number and Hartman number on fluid flow and heat transfer characteristics are studied in [18]. The results of [18] show that the average Nusselt number increases and average Poiseuille number decreases by adding the nano-particles to the base fluid. Transient, laminar, natural-convection flow of a micropolar-nanofluid (Al2O3/water) in the presence of a magnetic field in an inclined rectangular enclosure is considered in [19]. Authors show that circulation and convection become stronger by increasing Rayleigh and microrotation numbers but they are significantly suppressed by the presence of a strong magnetic field. In [20] heat transfer and fluid flow analysis in a straight channel utilizing nano-fluid are numerically studied, while flow field is under magnetic field. Usage of nano-particles in the base fluid and also applying magnetic field transverse to fluid velocity are two ways recommended in this paper to enhance heat exchange in straight duct.

Influence of external magnetic source to two-dimensional $Fe_3O_4$–water nanomaterial in a half circular shape cavity and semi annulus enclosure with sinusoidal hot wall are numerically addressed in [21, 22] and numerical solution is carried out using control volume based finite element method (CVFEM). It has been found that augmenting nanofluid volume fraction, Rayleigh and magnetic numbers leads to improve of the temperature gradient while it reduces with augment of Lorentz forces. The natural convection of CuO-water nanofluid flow and heat transfer in a cavity which is heated from below under the magnetic field effect is proposed in [23], and the governing equations are solved using the lattice Boltzmann method. Their results have indicated that enhancement in heat transfer has direct relationship with Hartmann number and heat source length but it has reverse relationship with Rayleigh number.

In [24] MHD mixed convection in a CuO-nanofluid filled lid-driven cavity having an elastic side wall and volumetric heat generation is numerically investigated. The left vertical wall moves with constant velocity in +y direction. The left vertical wall of the cavity is maintained at constant cold temperature while the right vertical wall is at hot temperature and the other walls of the cavity are insulated. Better thermal transport of the fluid within the cavity is seen due to the increment of effective thermal conductivity of the nanofluid as the volume fraction of the solid nanoparticles increases. Authors in [25, 26] propose mixed convection and MHD natural convection flow numerical study in a flexible sided, partially heated fluid-filled (and nanofluid-filled) triangular cavity with internal heat generation.

Influence of an inclined uniform magnetic field on mixed convection in an oscillating lid-driven cavity filled with nanofluid is numerically investigated in [27]. The cavity is heated from below and cooled from above while side walls are assumed to be adiabatic. The top wall velocity varies sinusoidally while no-slip boundary conditions are imposed on the other walls of the cavity. Their results have shown that the convection within the cavity is suppressed when the strength of the magnetic field is higher such that the corresponding Hartmann number is greater than 20. Authors in [28] also numerically studied the mixed convection of CuO–water nanofluid filled lid driven cavity having its upper and lower triangular domains under the influence of inclined magnetic fields. The top horizontal wall of the cavity moves with constant speed in +x direction while no-slip boundary conditions are imposed on the other walls. The top wall of the cavity has constant cold temperature while the bottom wall is at hot temperature and the other walls of the cavity are adiabatic. In [29] MHD free convection has been proposed in an inclined wavy enclosure filled with a Cu-water nanofluid in the presence of an isothermal corner heater and an inclined uniform magnetic field. The cavity is heated from the left bottom corner and cooled from the top wavy wall while the rest walls are adiabatic. It has been found that the heat transfer rate increases with nanoparticles volume fraction and variation of the cavity inclination angle leading to essential changes in the fluid flow and heat transfer.

The conjugate effect of Joule heating and magnetic field on MHD natural convection and the entropy generation are studied numerically inside a sinusoidal heated lid-driven cavity filled by Fe3O4-water nanofluid in [30]. It is shown that the increase of both Hartmann and Eckert number results in a decrease and increase in average Nusselt number and the entropy generation, respectively. The effect of inclination angle on the heat transfer of Al2O3–water nanofluid for mixed convection flows in a partially heated double lid driven inclined cavity is numerically simulated in [31]. At the lower wall of the cavity, two heat sources are fixed with the condition that the remaining part of the bottom wall is kept insulated. Top wall and vertically moving walls are maintained at constant cold temperature. Authors in [32] also studied entropy generation in the same configuration in [31] under the influence of inclined magnetic field.

The unsteady MHD mixed convection flows of SWCNT-water and Au-water nanofluids are investigated within a horizontal grooved channel with two heat generating solid cylinders in reference [33]. It has been found that the fluid flow and temperature are significantly affected by groove area and groove shape. On the other hand, the heat transfer rate is shown to be higher in the case of the Au-water nanofluid at low Reynolds number, but at high Reyolds number, the heat transfer rate is higher in the case of the SWCNT-water nanofluid. The constant magnetic field and slip effects on developing laminar forced convection of the mixture of FMWNT carbon nanotubes suspended in water in the microchannels are proposed in [34]. Slip velocity is supposed as the hydrodynamic boundary condition while the microchannel's lower wall is insulated and the top wall is under the effect of a constant heat flux.

The inclined magnetic field effect on mixed convection in Cu-water nanofluid filled lid-driven cavity is examined in [35]. Slip velocity is considered along the lid horizontal walls and a constant heat flux source is supposed on the left wall, meanwhile the right vertical wall is cooled isothermally. The remainder walls are thermally insulted. They show that the orientation of the magnetic field can be considered as a key control of the convective heat transfer where the suppression used by the magnetic field on the Nusselt number decreases by increasing the orientation of the applied magnetic field. Authors in reference [36] consider the effects of magnetic field on the flow field, heat transfer and entropy generation in a Cu-water nanofluid filled trapezoidal enclosure. The top wall of the enclosure is cold and moves toward right (or left) and the bottom wall is hot and the side walls are insulated. In [37] the effect of an external oriented magnetic field on heat transfer and entropy generation of Cu-water nanofluid flow in an open cavity heated from below is also investigated and the governing equations are solved numerically by finite-volume method. Authors in [38-43] have also proposed entropy generation, natural convection, MHD free and mixed convection and heat transfer of Cu-Water, CuO-Water and Water–$Fe_3O_4$ nanofluids in a C-shaped cavity and lid-driven square porous enclosure with partial slip and heat sink.

Although considerable papers have studied heat transfer enhancement of nanofluid in a square cavity, but based on the discussion about the literature and the author's best knowledge, the problem of MHD mixed convection inside a lid driven cavity filled by nanofluid, with internal Joule heating and volumetric heat generation has not been proposed. In addition, no proper study is found in the literature which uses the streamfunction-velocity formulation for numerical simulation of nanofluid filled cavity. Therefore, in this paper the effects of magnetic field, Joule heating and volumetric heat generation are investigated on heat transfer and fluid flow in a Cu-Water nanofluid filled lid driven cavity using enhanced streamfunction–velocity method. The dimensionless governing equations are solved numerically for the stream function and temperature using finite difference method for various Richardson($Ri$), Reynolds($Re$), Hartmann ($Ha$), Eckert($Ec$)numbers, magnetic field angle($\alpha$) and solid volume fraction of the nanofluid($\phi$) in MATLAB software. To discrete the streamfunction-velocity formulation five point constant coefficient second-order compact finite difference approximations are used which avoids difficulties inherent in the conventional streamfunction–vorticity and primitive variable formulations. The stream function equation is solved using fast Poisson's equation solver on a rectangular grid (POICALC function in MATLAB) and the temperature equation is solved using Jacobi bi-conjugate gradient stabilized (BiCGSTAB) method. The paper is organized as follows: Section 2 describes the problem geometry and mathematical formulations. Discretizations of the governing equations and the solution method are presented in section 3. Grid independency test and code validation are brought in section 4. Results and discussion are provided in detail in section 5. Finally, conclusion is in section 6.

## PROBLEM GEOMETRY AND MATHEMATICAL FORMULATIONS

The geometry of the problem is schematically shown in Fig. 1. The inclined constant magnetic field with flux density $B$ is applied, with respect to the coordinate system. The top and bottom walls of the cavity are adiabatic, and the side walls are kept at a constant temperature $T=T_c$. The top horizontal wall of the cavity moves with constant speed in +x direction while no-slip boundary conditions are imposed on the other walls (table 1). The cavity is filled with Cu- water nanofluid under the influence of the inclined magnetic field. Thermo-physical properties of water and copper at the reference temperature are presented in table 2. The nano-fluid is taken to be Newtonian, incompressible and laminar and the nano-particles are assumed to have a uniform shape and size. Moreover, it is assumed that both the fluid phase and nano-particles are in thermal equilibrium state and the slip velocity between the phases is ignored. Therefore, nano-fluid is modeled with single phase approach. In the other hand, the buoyancy force in the momentum equation is approximated by using the Boussinesq approximation. Thus Continuity, momentum and energy equations in scalar form considering internal joule heating effect and volumetric heat generation in two dimensional Cartesian coordinate system are written as follows:

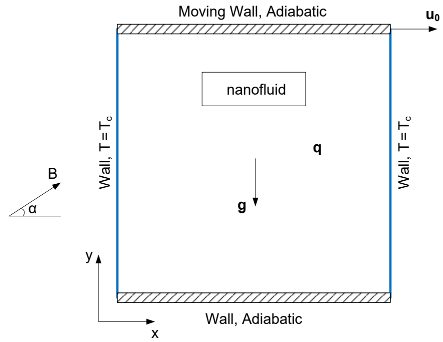


**Figure 1.** Geometry and the coordinate system

**Table 1.** Boundary conditions in Fig.1

| | Velocity | Temperature |
|---|---|---|
| Left wall | $v_x = v_y = 0$ | $T=T_c$ |
| Right wall | $v_x = v_y = 0$ | $T=T_c$ |
| Lower Wall | $v_x = v_y = 0$ | Adiabatic |
| Upper wall | $v_x = u_0$, $v_y = 0$ | Adiabatic |

**Table 2.** Thermo-physical properties

| Property | Water | Cu |
|---|---|---|
| $\rho$ (kg·m$^{-3}$) | 997.1 | 8933 |
| $C_p$(J·kg$^{-1}$·K$^{-1}$) | 4179 | 385 |
| $k$(W·m$^{-1}$·K$^{-1}$) | 0.613 | 401 |
| $\beta$( K$^{-1}$) | 2.1e-4 | 1.67e-5 |
| $\sigma$( mho·m$^{-1}$) | 0.05 | 5.97e7 |
| $\mu$( kg·m$^{-1}$·s$^{-1}$) | 1.003e-3 | --- |

$$\frac{\partial v_x}{\partial x} + \frac{\partial v_y}{\partial y} = 0 \tag{1}$$

$$-\mu_{nf}\left(\frac{\partial^2 v_x}{\partial x^2} + \frac{\partial^2 v_x}{\partial y^2}\right) + \rho_{nf}\left(v_x \frac{\partial v_x}{\partial x} + v_y \frac{\partial v_x}{\partial y}\right) = -\frac{\partial p}{\partial x} - \sigma_{nf} B_y\left(v_x B_y - v_y B_x\right) \tag{2}$$

$$-\mu_{nf}\left(\frac{\partial^2 v_y}{\partial x^2} + \frac{\partial^2 v_y}{\partial y^2}\right) + \rho_{nf}\left(v_x \frac{\partial v_y}{\partial x} + v_y \frac{\partial v_y}{\partial y}\right) = -\frac{\partial p}{\partial y} + (\rho\beta)_{nf} g_y (T - T_c) + \sigma_{nf} B_x\left(v_x B_y - v_y B_x\right) \tag{3}$$

$$-k_{nf}\left(\frac{\partial^{2} T}{\partial x^2} + \frac{\partial^2 T}{\partial y^2}\right) + \left(\rho C_p\right)_{nf}\left(v_x \frac{\partial T}{\partial x} + v_y \frac{\partial T}{\partial y}\right) = \sigma_{nf}\left(v_x B_y - v_y B_x\right)^2 + q \tag{4}$$

where $v_x$ and $v_y$are the velocity in the x any y directions, $B_x$and $B_y$ are the magnetic flux density in the x any y directions, $p$ is the pressure, $T$ is the temperature and $g_y$ is the gravitational acceleration in y direction. $\rho_{nf}$, $\mu_{nf}$, $k_{nf}$ ,

$(C_p)_{nf}$ and $\sigma_{nf}$are the density, the viscosity, the thermal conductivity, the specific heat and the electrical conductivity of the nanofluid respectively. $q$ is volumetric heat density. The terms $-\sigma_{nf}B_y(v_xB_y - v_yB_x)$ and $+\sigma_{nf}B_x(v_xB_y - v_yB_x)$appearing in (2) and (3), respectively, represent the Lorentz force per unit volume in the x and y directions and occur due to the electrical conductivity of the fluid. Also the term $\sigma_{nf}(v_xB_y - v_yB_x)^2$in (4) represents the Joule heating. The effective density, specific heat, thermal expansion coefficient and electrical conductivity of nanofluid are given by the following formulas [25]:

$$\rho_{nf} = (1-\phi)\rho_f + \phi\rho_s \tag{5}$$

$$(\rho C_p)_{nf} = (1-\phi)(\rho C_p)_f + \phi(\rho C_p)_s \tag{6}$$

$$(\rho\beta)_{nf} = (1-\phi)(\rho\beta)_f + \phi(\rho\beta)_s - \phi(1-\phi)(\rho_s - \rho_f)(\beta_s - \beta_f) \tag{7}$$

$$\sigma_{nf} = \left(1 + \frac{3(\sigma_s - \sigma_f)\phi}{(\sigma_s + 2\sigma_f) - (\sigma_s - \sigma_f)\phi}\right)\sigma_f \tag{8}$$

$$k_{nf} = k_{static} + k_{\text{Brownian}} \tag{9}$$

$$k_{static} = k_f + k_s \frac{d_f\phi}{d_s(1-\phi)} \tag{10}$$

$$k_{\text{Brownian}} = 36000 k_s \frac{U_s d_s}{k_f}(\rho C_p)_f \frac{d_f\phi}{d_s(1-\phi)} \tag{11}$$

$$U_s = \frac{2k_bT}{\pi\mu_f d_s^2} \tag{12}$$

The equation (11) is for nanofluids containing spherical nanoparticles with volume fraction between1% to 8% and base fluid could be water or ethylene glycol. $U_s$ is The Brownian motion velocity. $d_f$ and $d_s$ are the water molecules and copper nanoparticles diameter ($d_f$=2×10$^{-10}$ and $d_s$=100×10$^{-9}$). The effective viscosity of the nanofluid is given by [27]:

$$\mu_{nf} = \mu_{st} + \mu_{\text{Brownian}} = \frac{\mu_f}{(1-\phi)^{2.5}} + \frac{k_{\text{Brownian}}}{k_f} \times \frac{\mu_f}{Pr_f} \tag{13}$$

The continuity, momentum, and energy equations are expressed in the non-dimensional form using the following dimensionless parameters:

$$X = \frac{x}{L} \;, Y = \frac{y}{L} \;, V_x = \frac{v_x}{u_0}, V_y = \frac{v_y}{u_0}, P = \frac{p}{\rho_f u_0^2}, \theta = \frac{k_f \Delta T}{L^2 q}, Pr = \frac{(\mu C_p)_f}{k_f}, Gr = \frac{\rho_f^2 g_y \beta_f L^5 q}{k_f \mu_f^2}$$
$$, Re = \frac{\rho_f u_0 L}{\mu_f}, Ha = \sqrt{B_x^2 + B_y^2}\, L\sqrt{\frac{\sigma_f}{\mu_f}}, Ec = \frac{u_0^2}{C_{pf}\Delta T}, Ri = \frac{Gr}{Re^2} \tag{14}$$

Where dimensionless numbers *Pr*, *Gr*, *Re*, *Ha* , *Ec* and *Ri* are Prandtl, Grashof, Reynolds, Hartmann , Eckert and Richardson numbers, respectively. Therefore, dimensionless form of the governing equations can be expressed as:

$$\frac{\partial V_x}{\partial X}+\frac{\partial V_y}{\partial Y}=0 \tag{15}$$

$$\begin{aligned}-\frac{1}{Re}\frac{\mu_{nf}}{\mu_f}\left(\frac{\partial^2 V_x}{\partial X^2}+\frac{\partial^2 V_x}{\partial Y^2}\right)+\frac{\rho_{nf}}{\rho_f}\left(V_x\frac{\partial V_x}{\partial X}+V_y\frac{\partial V_x}{\partial Y}\right)\\ =-\frac{\partial P}{\partial X}-\frac{\sigma_{nf}}{\sigma_f}\frac{Ha^2}{Re}\left(V_x\frac{B_y^2}{|B|^2}-V_y\frac{B_xB_y}{|B|^2}\right)\end{aligned} \tag{16}$$

$$\begin{aligned}-\frac{1}{Re}\frac{\mu_{nf}}{\mu_f}\left(\frac{\partial^2 V_y}{\partial X^2}+\frac{\partial^2 V_y}{\partial Y^2}\right)+\frac{\rho_{nf}}{\rho_f}\left(V_x\frac{\partial V_y}{\partial X}+V_y\frac{\partial V_y}{\partial Y}\right)\\ =-\frac{\partial P}{\partial Y}+\frac{(\rho\beta)_{nf}}{(\rho\beta)_f}Ri\theta+\frac{\sigma_{nf}}{\sigma_f}\frac{Ha^2}{Re}\left(V_x\frac{B_xB_y}{|B|^2}-V_y\frac{B_x^2}{|B|^2}\right)\end{aligned} \tag{17}$$

$$\begin{aligned}-\frac{k_{nf}}{k_f}\left(\frac{\partial^2\theta}{\partial X^2}+\frac{\partial^2\theta}{\partial Y^2}\right)+\frac{\left(\rho C_p\right)_{nf}}{\left(\rho C_p\right)_f}Re\cdot Pr\left(V_x\frac{\partial\theta}{\partial X}+V_y\frac{\partial\theta}{\partial Y}\right)\\ =\frac{\sigma_{nf}}{\sigma_f}Ec\cdot Pr\cdot Ha^2\left(V_x\frac{B_y}{|B|}-V_y\frac{B_x}{|B|}\right)^2+1\end{aligned} \tag{18}$$

## SOLUTION METHOD

The typical difficulty of the stream-function-vorticity formulation is the lack of the simple physical boundary conditions for the vorticity field at the no-slip boundaries. In order to avoid the drawbacks associated with the vorticity values at the boundary, the streamfunction-velocity or the stream-function formulation-based methodology for the solution of the 2D incompressible fluid flows, which eliminates the need to calculate the vorticity as a part of the computational process, has been utilized for solving Navier-Stokes equations. The stream-function formulation includes the stream function and its first derivatives resulting in a fourth-order differential equation in stream function. The boundary conditions for stream function and velocities are generally known and are easy to be implemented computationally; thus the computational schemes are found to be very efficient. When the stream-function-velocity formulation, which is a fourth-order partial differential equation, is solved by finite differences, a uniform grid with 13 points must be needed to obtain a classical second-order finite difference approximation. This difference discretization using 13 grid points needs to be modified at grid points near the boundaries and must bring about difficulties for the solution of the resulting linear systems. In order to overcome the above drawback, the stream-function ($\Psi$) is established on a uniform grid using the four nearest neighbors' values of $\Psi$ and is the constant coefficient second-order compact scheme.

In this paper, an efficient compact finite difference approximation (five point constant coefficient second-order compact (5PCC-SOC) scheme), is used for the stream-function formulation of the steady incompressible Navier–Stokes equations, in which the grid values of stream-function and the values of its first derivatives (velocities) are carried as the unknown variables. Stream function is defined as:

$$V_x=\frac{\partial\Psi}{\partial Y} \tag{19}$$

$$V_y=-\frac{\partial\Psi}{\partial X} \tag{20}$$

Therefore, from (15) to (17) we have the following streamfunction–velocity formulation:

$$
\begin{aligned}
-\frac{1}{Re}\frac{\mu_{nf}}{\mu_f}\left(\frac{\partial^4\Psi}{\partial X^4}+2\frac{\partial^4\Psi}{\partial X^2\partial Y^2}+\frac{\partial^4\Psi}{\partial Y^4}\right)
&=\frac{\rho_{nf}}{\rho_f}\left[V_x\left(\frac{\partial^3\Psi}{\partial X^3}+\frac{\partial^3\Psi}{\partial X\partial Y^2}\right)+V_y\left(\frac{\partial^3\Psi}{\partial X^2\partial Y}+\frac{\partial^3\Psi}{\partial Y^3}\right)\right]+\frac{(\rho\beta)_{nf}}{(\rho\beta)_f}Ri\frac{\partial\theta}{\partial X} \\
&+\frac{\sigma_{nf}}{\sigma_f}\frac{Ha^2}{Re}\left[\left(\frac{\partial V_x}{\partial Y}\frac{B_y^2}{|B|^2}-\frac{\partial V_y}{\partial X}\frac{B_x^2}{|B|^2}\right)+\left(\frac{\partial V_x}{\partial X}-\frac{\partial V_y}{\partial Y}\right)\frac{B_xB_y}{|B|^2}\right]
\end{aligned} \tag{21}
$$

Equations 21 and 18 are solved with the dimensionless boundary conditions $\Psi=0$ at all walls, $\theta=0$ at the side walls, and $\frac{\partial\theta}{\partial Y}=0$ at the top and bottom walls. Some standard finite difference operators at mesh point ($x_i$,$y_j$) are given by[45]:

$$
\begin{aligned}
\delta_x^2\delta_y\Psi &= \frac{\Psi_5+\Psi_6-\Psi_7-\Psi_8-2(\Psi_2-\Psi_4)}{2h^3} \\
\delta_x\delta_y^2\Psi &= \frac{\Psi_5-\Psi_6-\Psi_7+\Psi_8-2(\Psi_1-\Psi_3)}{2h^3} \\
\delta_x^2\Psi &= \frac{\Psi_1-2\Psi_0+\Psi_3}{h^2} \\
\delta_y^2\Psi &= \frac{\Psi_2-2\Psi_0+\Psi_4}{h^2} \\
\delta_x\Psi &= \frac{\Psi_1-\Psi_3}{2h} \\
\delta_y\Psi &= \frac{\Psi_2-\Psi_4}{2h}
\end{aligned} \tag{22}
$$

Where subscript 0 refers to the point ($x_i$,$y_j$) in the cavity, while *h* is the grid spacing. We can obtain the following relations at an interior grid point ($x_i$,$y_j$) for a sufficiently smooth solution Ψ using the Taylor series[45]:

$$
\begin{aligned}
\delta_x^2\Psi &= \frac{\partial^2\Psi}{\partial X^2}+\frac{h^2}{12}\frac{\partial^4\Psi}{\partial X^4}+O(h^4) \\
\delta_x\Psi_x &= \frac{\partial^2\Psi}{\partial X^2}+\frac{h^2}{6}\frac{\partial^4\Psi}{\partial X^4}+O(h^4) \\
\delta_y^2\Psi &= \frac{\partial^2\Psi}{\partial Y^2}+\frac{h^2}{12}\frac{\partial^4\Psi}{\partial Y^4}+O(h^4) \\
\delta_y\Psi_y &= \frac{\partial^2\Psi}{\partial Y^2}+\frac{h^2}{6}\frac{\partial^4\Psi}{\partial Y^4}+O(h^4) \\
\frac{\partial^4\Psi}{\partial X^2\partial Y^2} &= \frac{\partial^3\Psi}{\partial X\partial Y^2}=\delta_x\delta_y^2\Psi_x+O(h^2) \\
\frac{\partial^4\Psi}{\partial X^2\partial Y^2} &= \frac{\partial^3\Psi}{\partial X^2\partial Y}=\delta_x^2\delta_y\Psi_y+O(h^2)
\end{aligned} \tag{23}
$$

We can obtain from (23):

$$
\begin{aligned}
\frac{\partial^4\Psi}{\partial X^4} &= \frac{12}{h^2}\left(-\delta_x^2\Psi+\delta_x\Psi_x\right)+O(h^2)=\frac{12}{h^2}\left(-\delta_x^2\psi-\delta_xV_y\right)+O(h^2) \\
\frac{\partial^4\Psi}{\partial Y^4} &= \frac{12}{h^2}\left(-\delta_y^2\Psi+\delta_y\Psi_y\right)+O(h^2)=\frac{12}{h^2}\left(-\delta_y^2\Psi+\delta_yV_x\right)+O(h^2) \\
\frac{\partial^4\Psi}{\partial X^2\partial Y^2} &= \frac{1}{2}\left(\delta_x\delta_y^2\Psi_x+\delta_x^2\delta_y\Psi_y\right)+O(h^2)=\frac{1}{2}\left(-\delta_x\delta_y^2V_y+\delta_x^2\delta_yV_x\right)+O(h^2)
\end{aligned} \tag{24}
$$

Substituting (24) into (21) and using (22), and omitting the truncation error, we can obtain the following second-order compact finite difference formulation:

$$
\begin{aligned}
48\Psi_0 - 12\sum_{k=1}^{4}\Psi_k = 6h\left(V_{y1} - V_{y3} - V_{x2} + V_{x4}\right) + h^4\left(\delta_x\delta_y^2 V_y - \delta_x^2\delta_y V_x\right) \\
+\frac{\mu_f}{\mu_{nf}}\frac{\rho_{nf}}{\rho_f} Reh^2\left(V_{y0}\sum_{k=1}^{4}V_{xk} - V_{x0}\sum_{k=1}^{4}V_{yk}\right) \\
+\frac{\mu_f}{\mu_{nf}}\frac{(\rho\beta)_{nf}}{(\rho\beta)_f} ReRih^4\frac{\partial\theta}{\partial X} \\
+\frac{\mu_f}{\mu_{nf}}\frac{\sigma_{nf}}{\sigma_f} Ha^2h^4\left[\left(\delta_y^2\Psi\frac{B_y^2}{|B|^2} + \delta_x^2\Psi\frac{B_x^2}{|B|^2}\right) + \left(\delta_x V_x - \delta_y V_y\right)\frac{B_x B_y}{|B|^2}\right]
\end{aligned}
\qquad (25)
$$

Fourth order compact approximations for $V_x$ and $V_y$ are given, respectively, by [45]:

$$\frac{1}{6}V_{x2} + \frac{4}{6}V_{x0} + \frac{1}{6}V_{x4} = \frac{\Psi_2 - \Psi_4}{2h} \qquad (26)$$

$$\frac{1}{6}V_{y1} + \frac{4}{6}V_{y0} + \frac{1}{6}V_{y3} = \frac{\Psi_3 - \Psi_1}{2h} \qquad (27)$$

The sequence of the algorithm is provided here:
1. Assuming the value of the velocity and the stream function fields (for example zero).
2. Solving the discrete temperature equation, using Jacobi BiCGSTAB method.
3. Solving the discrete stream function equation (eq.25), using fast Poisson's equation solver on a rectangular grid (POICALC function) in MATLAB.
4. Calculating the velocity field from equations 26 and 27, using the stream function field and tri-diagonal matrix solver (tridiag function) in MATLAB.
5. Checking error in temperature and stream function fields. If errors are below the specified tolerance, exit the loop, otherwise, return to step 2. Repeat the whole procedure till converged solution is obtained. The tolerance of the convergence criterion used for all variables is $10^{-7}$:

$$|\theta^{k+1} - \theta^{k}| \leq 10^{-7} \qquad (28)$$

$$|\Psi\text{^}(k+1) - \Psi\text{^}k\,| \leq 〖10〗\text{^}(-7) \qquad (29)$$

### Grid independency test and validation

A grid independence test is performed for this study, with $Pr$=6.837, $Gr$=$10^6$, $Re$=100, $Ha$=100, $Ec$=0, $\phi$= 0.05 and α=45° (angle of flux density B) in order to determine the proper grid size. The following seven mesh-grid sizes are considered for the grid independence study. These mesh-grid densities are 40×40, 64×64, 80×80, 100×100, 128×128, 144×144 and 160×160. The maximum temperature $\theta_{max}$, the maximum stream function $\Psi_{max}$ of the fluid and the averaged Nusselt number $Nu_{avg}$ on the right side wall of the cavity are used as a sensitivity measure of the solution accuracy, and are selected as the monitoring variables for the grid independence study. Table 3 shows the dependence of the quantities $\theta_{max}$, $\Psi_{max}$ and $Nu_{avg}$ on the grid size. Considering the accuracy of the numerical values, the following calculations are performed with structural uniform quadrilateral (square) 128×128 grid. The numerical code is benchmarked with a differently heated cavity problem filled with pure fluid, which is maintained at cooled condition, by the right wall. The left wall is hot, whereas the two horizontal walls are under adiabatic condition. The governing equations are solved on a uniform grid and for the Prandtl number, $Pr$ = 0.71. The solutions are obtained for different values of Rayleigh number and $Ha$=0. Comparisons of some relevant flow and heat transfer parameters with the corresponding literature data for different approaches are reported in Table 4. The parameters considered are the maximum value of the horizontal velocity component ($V_{xmax}$) on the vertical mid-plane ($X$ = 0.5); the maximum value of the vertical velocity component ($V_{ymax}$) on the horizontal mid-plane ($Y$ = 0.5) and $Nu_{avg}$ values on the heated side wall ($X$ = 0). The obtained results of the proposed code show an acceptable agreement with the others.

Furthermore, the present solver is validated against the existing numerical results of [20, 28, 54, 55]. The comparison of streamline contours and isotherm lines obtained from the present code and those of [20, 28, 54, 55] for natural convection through the enclosure under magnetic field are shown in Fig.2 for ($Ra$=7000 and $Ha$=25) and ($Ra$=7×$10^5$ and $Ha$=100). Comparisons confirm agreement accuracy with those of the literature.

**Table 3.** Different mesh-grid densities for $Pr$=6.837, $Gr$=$10^6$, $Re$=100, $Ha$=100, $Ec$=0, $\phi$= 0.05 and α=45°

| Grid size | $\theta_{max}$ | $\Psi_{max}$ | $Nu_{avg}$ | CPU Time(s) |
|---|---|---|---|---|
| 40×40 | 0.06649 | 0.00315 | 0.26909 | 9 |
| 64×64 | 0.06442 | 0.00306 | 0.37535 | 39 |
| 80×80 | 0.06134 | 0.00303 | 0.40888 | 72 |
| 100×100 | 0.05972 | 0.00299 | 0.43173 | 134 |
| 128×128 | 0.05849 | 0.00295 | 0.44821 | 269 |
| 144×144 | 0.05807 | 0.00294 | 0.45418 | 439 |
| 160×160 | 0.05773 | 0.00293 | 0.45830 | 584 |

**Table 4.** Comparison of the present results with those of [30, 40–47] for different $Ra$

| Rayleigh number | | $10^3$ | $10^4$ | $10^5$ | $10^6$ | $10^7$ |
|---|---|---|---|---|---|---|
| $V_{xmax}$ | Current study | 3.651 | 16.172 | 34.710 | 64.607 | 147.705 |
| | Ref. [30] | 3.645 | --- | 34.719 | --- | 148.511 |
| | Ref. [46] | 3.652 | 16.163 | 35.521 | 64.186 | 164.236 |
| | Ref. [47] | 3.636 | 16.167 | 34.962 | 64.133 | 148.768 |
| | Ref. [48] | 3.650 | 16.178 | 34.764 | 64.835 | 148.440 |
| | Ref. [49] | 3.634 | 16.134 | 34.662 | 64.511 | --- |
| | Ref. [50] | 3.648 | 16.183 | 34.741 | 64.830 | 148.569 |
| | Ref. [51] | --- | --- | 34.749 | 64.827 | 148.590 |
| | Ref. [52] | 3.650 | 16.203 | 34.825 | 65.332 | 155.820 |
| | Ref. [53] | --- | --- | --- | --- | 148.600 |
| $V_{ymax}$ | Current study | 3.696 | 19.601 | 68.504 | 220.099 | 694.949 |
| | Ref. [30] | 3.695 | --- | 68.590 | --- | 701.658 |
| | Ref. [46] | 3.682 | 19.569 | 68.655 | 219.866 | 701.922 |
| | Ref. [47] | 3.686 | 19.597 | 68.578 | 220.537 | 702.029 |
| | Ref. [48] | 3.698 | 19.625 | 68.603 | 220.533 | 699.571 |
| | Ref. [49] | 3.674 | 19.526 | 68.216 | 218.281 | --- |
| | Ref. [50] | 3.695 | 19.628 | 68.638 | 220.567 | 699.299 |
| | Ref. [51] | --- | --- | 68.646 | 220.630 | 699.670 |
| | Ref. [52] | 3.697 | 19.613 | 68.606 | 221.658 | 696.238 |
| | Ref. [53] | --- | --- | --- | --- | 699.200 |
| $Nu_{avg}$ | Current study | 1.117 | 2.243 | 4.520 | 8.804 | 16.495 |
| | Ref. [30] | --- | --- | --- | --- | --- |
| | Ref. [46] | 1.127 | 2.247 | 4.522 | 8.805 | 16.790 |
| | Ref. [47] | 1.117 | 2.246 | 4.518 | 8.792 | 16.408 |
| | Ref. [48] | 1.117 | 2.244 | 4.521 | 8.824 | 16.526 |
| | Ref. [49] | 1.138 | 2.264 | 4.544 | 8.837 | --- |
| | Ref. [50] | 1.117 | 2.244 | 4.519 | 8.821 | 16.510 |
| | Ref. [51] | --- | --- | 4.521 | 8.825 | 16.522 |
| | Ref. [52] | 1.118 | 2.243 | 4.512 | 8.763 | 16.075 |
| | Ref. [53] | --- | --- | --- | --- | 16.520 |

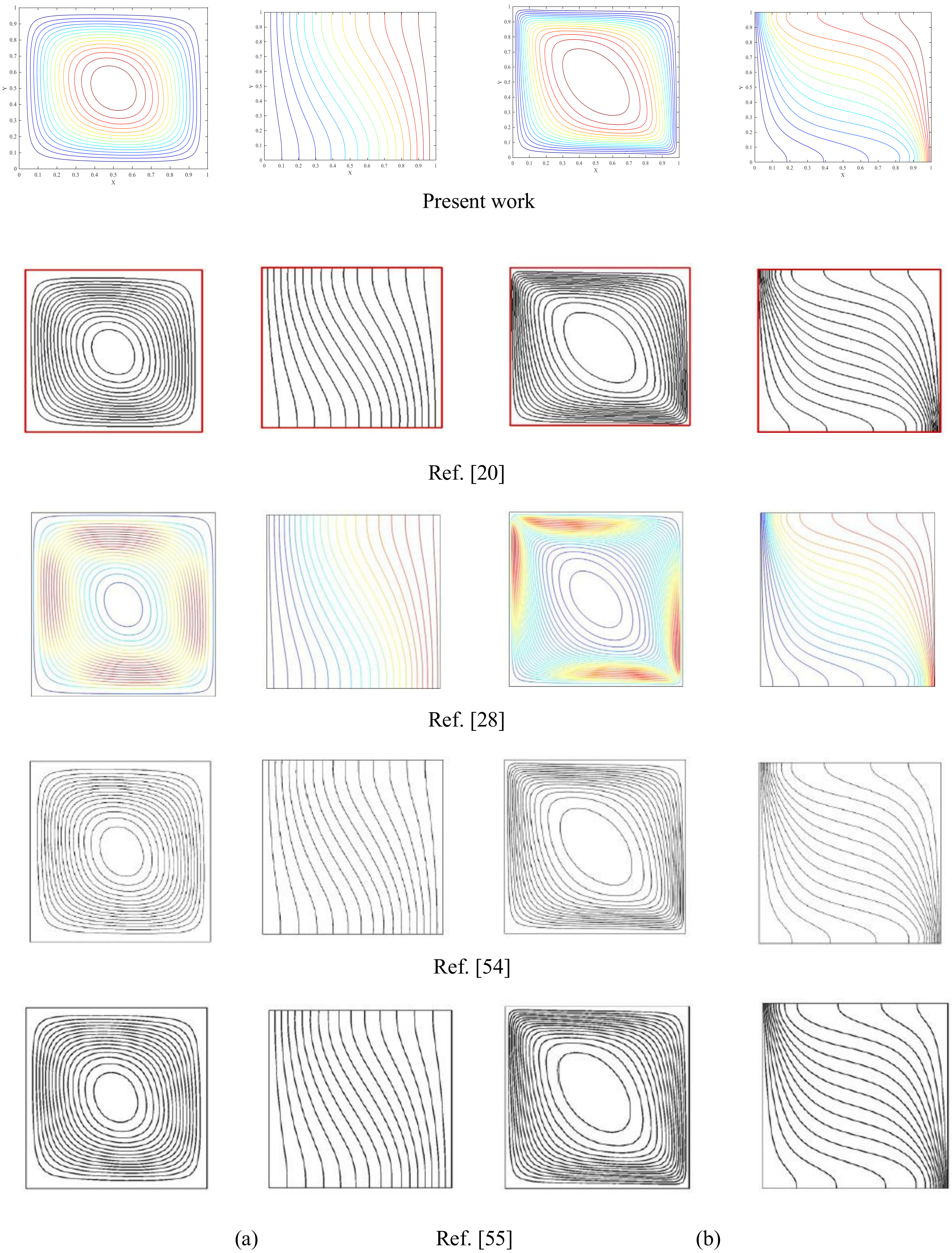


**Figure 2.** Streamlines and isotherms comparison of the present code with the results obtained from [20, 28, 54, 55] for: (a) $Ra$=7000 and $Ha$=25; (b) $Ra$=7×10$^5$ and $Ha$=100.

## Results and discussion

The natural and forced convection in a Cu-Water nanofluid filled lid driven cavity with volumetric heat generation, Joule heating and in the presence of an external magnetic field are considered in this study. Parametric numerical simulations are performed in the following range of parameter values: $10^4 \leq Gr \leq 10^7$; $0 \leq Re \leq 100$; $0 \leq Ha \leq 100$; $0 \leq Ec \leq 0.08$; $0 \leq \phi \leq 0.08$; $0 \leq \alpha \leq 135°$. The fluid flow and thermal fields are analyzed through the streamlines and isotherm contours. The heat transfer within the cavity is characterized by Nusselt number. The resulting Nusselt number for the cases under consideration $Nu_1$ is defined as $1/\theta_{max}$ [56].

## Effect of Richardson number

To study the influence of Richardson number, it is varied between $1 \leq Ri \leq 1000$, while $Re$=100, $Ha$= 0, $Ec$=0 and $0 \leq \phi \leq 0.08$. The effect of Richardson numbers on streamlines and isotherms are shown in Fig.3 and Fig.4. The ratio of natural to forced convection is measured by Richardson number. For low $Ri$ range ($Ri$=1) the forced convection is dominant. Figures 3(a) and 4(a) indicate that the buoyancy effect is overpowered by shear effect due to the movement of the top lid in lid-driven cavity. The streamlines behavior in the lid-driven cavity is distinguished by a primary re-circulating cell occupying most of the cavity generated by the lid. The flow due to the moving lid penetrates more into the cavity at low $Ri$. Furthermore, for value of $Ri$ = 10 mixed convection is dominant. Figures 3(b) and 4(b) point out the buoyancy effect has magnitude relatively comparable with the shear effect. The flow streamlines still show a primary re-circulating cell of the size of the cavity generated by the moving top lid and two secondary eddies near the bottom corners with the one near the left bottom corner bigger and stronger than the one in the right bottom corner of the cavity. The center of the primary cell moves towards the top moving wall. For values of $Ri$ = 100 and 1000 the buoyancy effect is dominant, the isotherms move towards the top wall, secondary recirculation zone near the left wall of the cavity can be seen, $\theta_{max}$ decreases, and the rotating vortices become larger. In this case the effect of natural convection becomes important and the convection is enhanced. The effect of internal heating becomes more important when $Ri$ is high and the isotherms become parallel to the horizontal walls indicating the dominance of convection inside the cavity. Figure 4 indicate that, an increase in solid volume fraction to 0.08 increases the values of $\Psi_{max}$. The effects of Richardson number and volume fraction of the nano-particles on the $Nu_1$ are shown in Fig. 5. It is clear that the $Nu_1$ significantly increases by increasing $Ri$ and $\phi$.

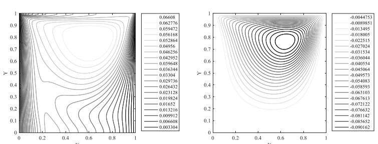

a) $Ri$=1

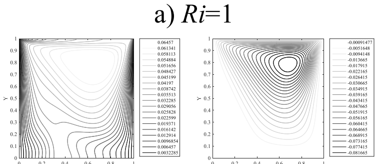

b) $Ri$=10

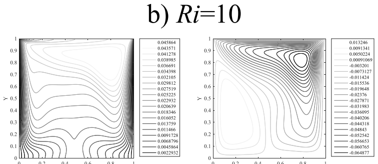

c) $Ri$=100

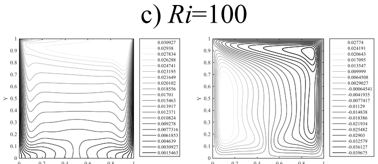

d) $Ri$=1000

**Figure 3.** Isotherms (left) and streamlines (right) contours at different $Ri$ and $Re$=100, $Ha$= 0, $Ec$=0, $\alpha$ =0°, $\phi$= 0

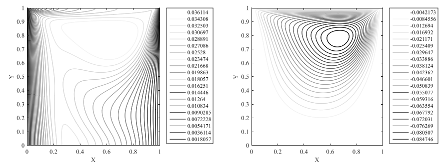

a) $Ri$=1

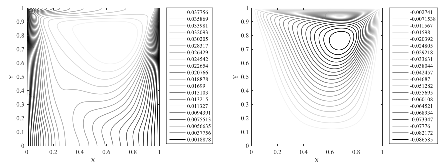

b) $Ri$=10

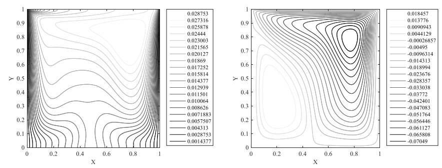

c) $Ri$=100

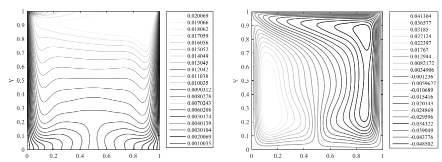

d) Ri=1000

**Figure 4.** Isotherms (left) and streamlines (right) contours at different $Ri$ and $Re$=100, $Ha$= 0, $Ec$=0, $\alpha$ =0°, $\phi$= 0.08

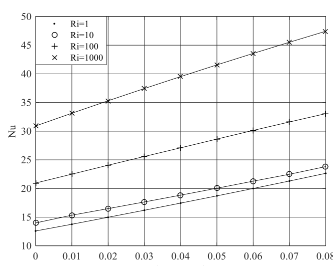


**Figure 5.** Variations of $Nu_1$ with $Ri$ and $\phi$ for $Re$=100, $Ha$= 0, $Ec$=0 and $\alpha$ =0°

### Effect of Reynolds number

To study the influence of Reynolds number, it is varied between 1≤ $Re$ ≤ 100, while $\alpha$ =0°, $Ha$=0, 0≤ $\phi$≤0.08 and $Ec$=0.04. Figures 6 and 7 show the effect of Reynolds number on isotherm and streamline contours. As can be noticed from these figures, for $Re$=1 the flow is almost symmetric along the vertical midline of the cavity and with two counter-rotating cells. Eddies become asymmetric, $\Psi_{max}$ decreases, and one eddy moves up toward the top wall by increasing the Reynolds number. As it can be observed from the isotherm plots at low Reynolds numbers ($Re$=1), the contours are almost parallel. However, more increasing of the Reynolds number enhances convective cooling. The isotherm contours change significantly and become asymmetric. The location of the maximum temperature moves down from the top wall of the cavity by increasing the Reynolds number. Effect of Reynolds number on Nusselt number with different nanoparticle volume fraction is shown in Fig. 8. It is observed that Nusselt number $Nu_1$ increases by increasing the nanoparticle volume fraction. But increase of $Re$ from 50 to 100 play a little role for enhancement of $Nu_1$ in a constant nanoparticle volume fraction.

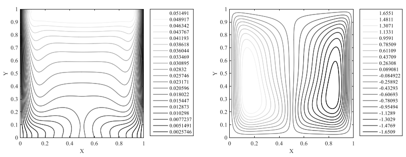

a)*Re*=1

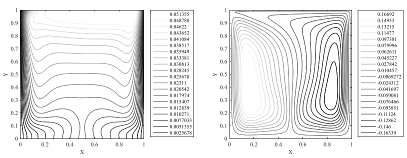

b)*Re*=10

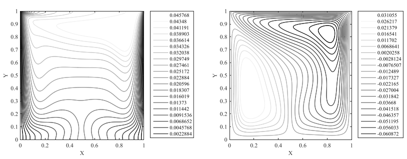

c)*Re*=50

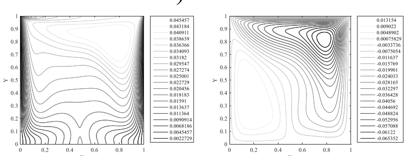

d)*Re*=100

**Figure 6.** Isotherms (left) and streamlines (right) contours at different Reynolds numbers and $Gr$=$10^6$, $Ha$= 0, $Ec$=0.04, $\alpha$ =0°, $\phi$= 0

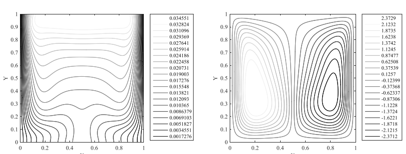

a)*Re*=1

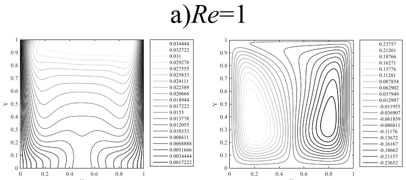

b)*Re*=10

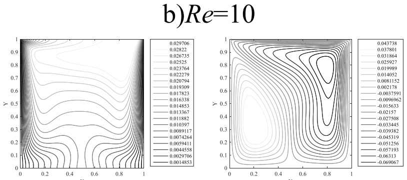

c)*Re*=50

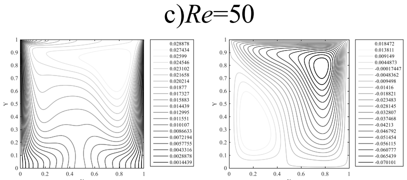

d)*Re*=100

**Figure 7.** Isotherms (left) and streamlines (right) contours at different Reynolds numbers and $Gr$=$10^6$, $Ha$= 0, $Ec$=0.04 and $\alpha$ =0°, $\phi$= 0.08

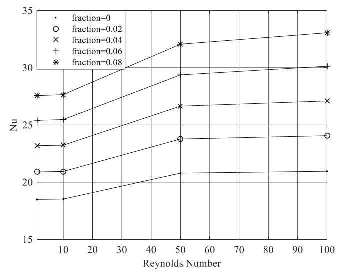


**Figure 8.**Variations of $Nu_l$ with $Re$ and $\phi$ for $Gr$=$10^6$, $Ha$= 0, $Ec$=0.04 and $\alpha$ =0°

## Effect of magnetic field orientation

To study the influence of magnetic field angle, it is considered 0≤ α ≤ 135°, 25≤ $Ha$ ≤100, while $Re$=100, $Gr$= $10^6$, $Ec$=0, $\phi$=0.04. Fig. 9 shows the isotherms and streamlines for various values of $\alpha$. It is shown that for α=0, streamlines are more clustered in the middle of the cavity and the isotherms are in the central parts of the cavity. When inclination angle is increased from 0 to 90, isotherms moves toward the top of the cavity and the streamlines are deformed from their original shape and the cluster of streamlines is shifted to the right vertical wall. Finally, for α=135°, the cluster of streamlines in the bottom of the cavity have the same direction of α. Impacts of magnetic field inclination angle and $Ha$ on $Nu_l$ are shown in Fig.10. It is observed that the $Nu_l$ decreases with the increase of $Ha$ and also increases for α= 90° at the same $Ha$.

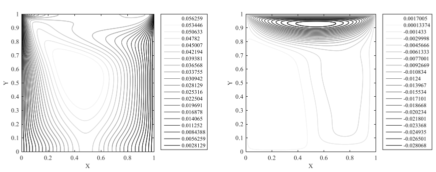

a) α=0°

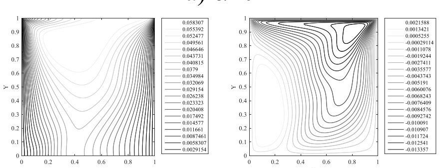

b) α=45°

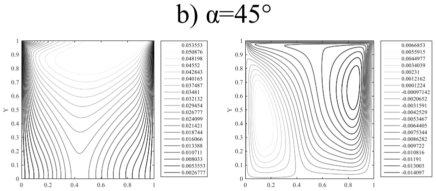

c) α=90°

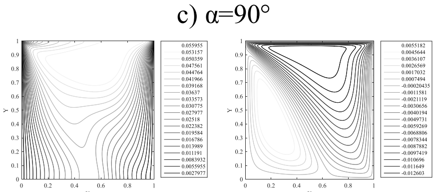

d) α=135°

**Figure 9.** Isotherms (left) and streamlines (right) contours at different magnetic field angles and $Gr$=$10^6$, $Re$= 100, $Ha$=100, $Ec$=0, $\phi$= 0.04

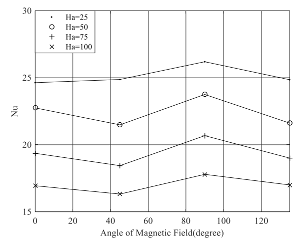


**Figure 10.** Variations of $Nu_1$ with magnetic field angle and $Ha$ for $Gr$=$10^6$, $Re$= 100, $Ec$=0 and $\phi$= 0.04

### Effect of Hartmann number

To study the influence of Hartmann number, it is considered $Ha$=25, 50, 75 and 100, while $Re$=100, $Gr$= $10^6$, $Ec$=0, $0\leq \phi \leq 0.08$ and α=0, 45°, 90°. Figures 11, 13 and 15 show the effect of Hartmann number on isotherm and streamline contours. It is clear that, Lorentz force will be generated perpendicularly to the direction of the applied magnetic field. Accordingly, the streamlines are weakened and secondary vortex is compressed to be limited close to the top wall. The isotherms are transmitted from convection model to vertical pattern by increasing $Ha$ due to the magnetic force effect which points out to the suppression of the convection. The existence of the metallic nanoparticles in the base fluid improves the thermal conductivity of the nanofluid and the thermal buoyancy forces are enhanced. Figure 11 shows that the isotherms start to move away from the top moving wall with increase of the Hartmann number. On the other hand, from figure 15 it can be seen that by increasing the magnetic field angle to 90° the clustering of the isotherm maps near the top wall is increased. The effects of Hartmann number and volume fraction of nano-particles on Nusselt number are shown in Figures 12, 14 and 16. The heat transfer within the cavity is decreased by increasing Hartmann number and conduction heat transfer is improved and so reduces $Nu_1$ value. On the other hand, it can be seen that increasing the magnetic field angle improves a small amount convective heat transfer across the cavity. In addition, as can be noticed from these figures, the presence of nanoparticles in the base fluid improves the heat transfer of nanofluid within the cavity compared to the pure fluid and increases $Nu_1$ value.

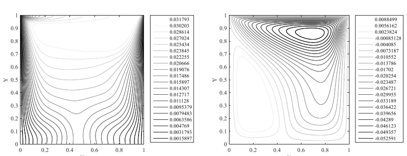

a) $Ha$=25

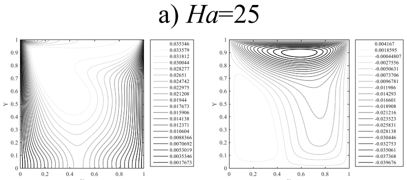

b) $Ha$=50

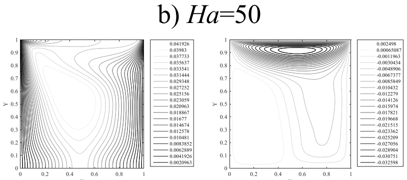

c) $Ha$=75

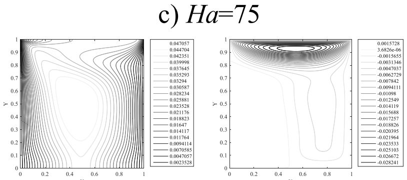

d) $Ha$=100

**Figure 11.** Isotherms (left) and streamlines (right) contours at different $Ha$, $Gr$=$10^6$, $Re$= 100, $Ec$=0,$\alpha$=0, $\phi$= 0.08

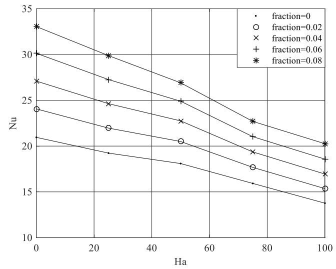


**Figure 12.** Variations of $Nu_1$ with $Ha$ for $Gr$=$10^6$, $Re$= 100, $Ec$=0 and $\alpha$= 0 at different $\phi$

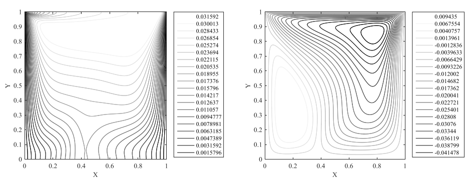

a) $Ha$=25

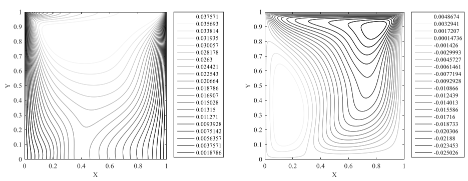

b) $Ha$=50

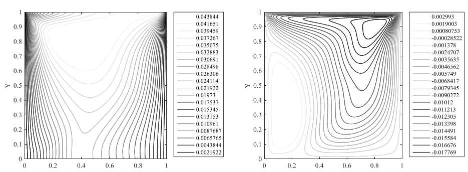

c) $Ha$=75

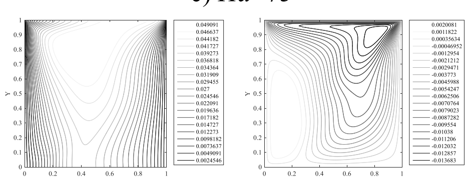

d) $Ha$=100

**Figure 13.** Isotherms (left) and streamlines (right) contours at different Ha, $Gr$=$10^6$, $Re$= 100, $Ec$=0, $\alpha$=45°, $\phi$= 0.08

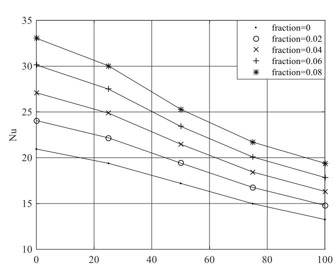


**Figure 14.** Variations of $Nu_1$ with $Ha$ for $Gr$=$10^6$, $Re$= 100, $Ec$=0 and $\alpha$= 45° at different $\phi$

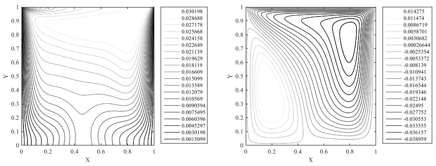

a) *Ha*=25

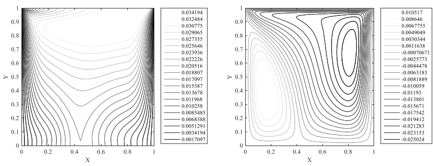

b) *Ha*=50

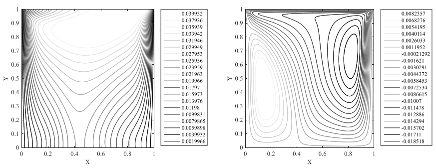

c) *Ha*=75

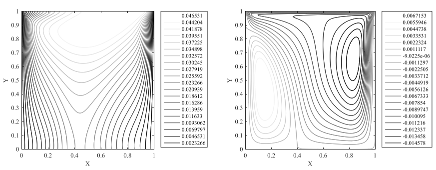

d) *Ha*=100

**Figure 15.** Isotherms (left) and streamlines (right) contours at different *Ha*, $Gr$=$10^6$, *Re*= 100, *Ec*=0, $\alpha$=90°, $\phi$= 0.08

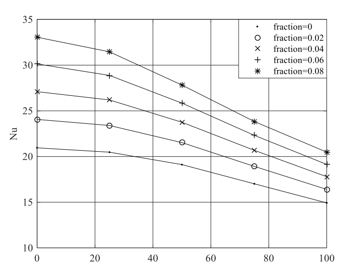


**Figure 16.**Variations of $Nu_l$ with *Ha* for $Gr$=$10^6$, *Re*= 100, *Ec*=0 and $\alpha$= 90° at different $\phi$

## Effect of Eckert number

To study the influence of Eckert number, it is varied between 0≤ $Ec$ ≤ 0.08, while *Re*=100, $Gr$= $10^6$, *Ha*=50, $\phi$=0.04 and 0≤ α ≤ 90°. Figure 17 shows the effect of Eckert number on isotherm and streamline contours. It can be observed that the size of the primary vortices enhances with increase of Eckert number due to the increase of the heat generation inside the cavity and when Eckert number is increased vortices becomes bigger. Isotherms start to move away from the left wall to the right wall of the cavity and convection is decreased by increasing Ec value, therefore, Joule heating has a negative effect on the convection within the cavity. The effects of Eckert number and magnetic field angle on Nusselt number is shown in Figure 18. It can be investigated that *Nu* is decreased by increasing Joule heating effect due to the strong distortion effect of Joule heating on convection current of heat transfer. It can also be seen that the Nusselt number is almost constant when magnetic field angle is varied between 70°<α<90° at a constant Eckert number.

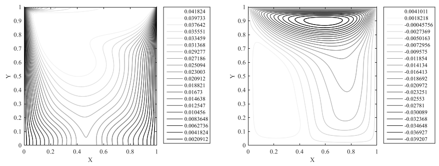

a) $Ec$=0

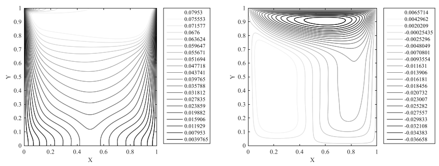

b) $Ec$=0.02

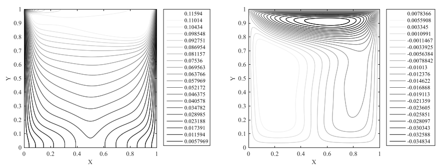

c) $Ec$=0.04

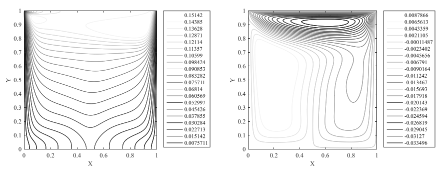

d) $Ec$=0.06

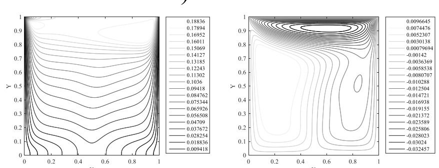

e) $Ec$=0.08

**Figure 17.** Isotherms (left) and streamlines (right) contours at different $Ec$, $Gr=10^6$, $Re$= 100, $Ha$=50, $\alpha$=0, $\phi$= 0.04

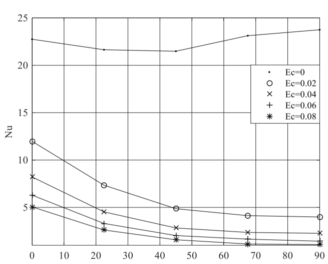


**Figure 18.** Variations of $Nu_1$ with magnetic field angle for $Gr=10^6$, $Re$= 100, $Ha$=50 and $\phi$=0.04 at different $Ec$

## CONCLUSION

This paper proposes the conjugate effect of volumetric heat generation, Joule heating and MHD natural convection on heat transfer and fluid flow in a Cu-Water nanofluid filled lid driven cavity. A fast and accurate streamfunction–velocity method is used to solve the governing equations of the problem. To discretize the streamfunction-velocity formulation five point constant coefficient second-order compact (5PCC-SOC) finite difference approximation is used. The stream function equation is solved using fast Poisson's equation solver on a rectangular grid (POICALC function in MATLAB) and temperature equation is solved using Jacobi bi-conjugate gradient stabilized (BiCGSTAB) method. The dimensionless governing equations are solved for Richardson number

$1 \leq Ri \leq 1000$, Reynolds number $0 \leq Re \leq 100$, Hartmann number $0 \leq Ha \leq 100$, Eckert number $0 \leq Ec \leq 0.08$, magnetic field angle $0 \leq \alpha \leq 135°$ and solid volume fraction of the nanofluid $0 \leq \phi \leq 0.08$. The present study leads to the following results:

- For low $Ri$ range ($Ri$=1) the forced convection is dominant. Furthermore, for value of $Ri$ = 10 mixed convection is dominant and for values of $Ri$ = 100 and 1000 the buoyancy effect is dominant, the isotherms move towards to the top wall, $\theta_{max}$ decreases, and the rotating vortices become larger.
- The Nusselt number is significantly increased by increasing Richardson number and solid volume fraction of the nanofluid.
- It can be observed from the isotherm plots at low Reynolds numbers ($Re$ = 1), the contours are almost parallel. However, more increasing of the Reynolds number enhances convective cooling. It is also observed that Nusselt number $Nu_1$ increases by increasing the nanoparticle volume fraction.
- Increasing the Reynolds number enhances convective cooling but, increase of $Re$ from 50 to 100 play a little role for enhancement of Nusselt number in a constant nanoparticle volume fraction.
- When inclination angle is increased from 0 to 90, isotherms moves toward the top of the cavity and the streamlines are deformed from their original shape and the cluster of streamlines is shifted to the right vertical wall. It is also observed that the $Nu_l$ decreases with the increase of $Ha$ and also increases for α= 90° at the same $Ha$.
- The isotherms are transmitted from convection model to vertical pattern by increasing $Ha$ due to the magnetic force effect which points out to the suppression of the convection. The existence of the metallic nanoparticles in the base fluid improves the thermal conductivity of the nanofluid and the thermal buoyancy forces are enhanced.
- The heat transfer within the cavity is decreased by increasing Hartmann number and so reduces $Nu_l$ value. On the other hand, it can be seen that increasing the magnetic field angle improves a small amount convective heat transfer across the cavity.
- Joule heating has a negative effect on the convection within the cavity and convection is decreased by increasing Eckert number. It can also be investigated that $Nu_l$ is decreased by increasing Joule heating effect. In addition, It can be seen that the Nusselt number is almost constant when magnetic field angle is varied between 70° < α < 90° at a constant Eckert number.

## NOMENCLATURE

B magnetic flux density vector: $Wb \cdot m^{-2}$
$C_p$ specific heat: $J.kg^{-1}K^{-1}$
$d$ particle size (diameter): m
$g$ gravitational acceleration vector: $m \cdot s^{-2}$
$h$ grid spacing: m
$k_b$ Boltzmann constant: $kg \cdot m^2 \cdot s^{-2} \cdot K^{-1}$
$k$ thermal conductivity: $W \cdot m^{-1} \cdot K^{-1}$
$L$ dimension of cavity: m
$p$ pressure: $N \cdot m^{-2}$
$q$ volumetric heat source density: $W \cdot m^{-3}$
$T$ temperature: K
$U_s$ Brownian motion velocity: $m \cdot s^{-1}$
$v$ velocity vector: $m \cdot s^{-1}$
$x, y, z$ Cartesian coordinates: m
Greek symbols
$\alpha$ angle of orientation of the magnetic field
$\beta$ coefficient of volumetric expansion: $K^{-1}$
$\phi$ relative nanoparticle volumetric fraction
$\mu$ dynamic viscosity: $kg.\ m^{-1}s^{-1}$
$\rho$ density: $kg.m^{-3}$
$\sigma$ electrical conductivity: $mho.m^{-1}$
$\Psi$ stream function: $m^2s^{-1}$
Subscript
0 reference value

c cold
*f* fluid
max maximum value
nf nanofluid
*s* nanoparticle
*st* static
*x, y, z* component of a vector quantity
Dimensionless quantities
*V* velocity vector
*P* Pressure
*X* Cartesian coordinate in *x* direction
*Y* Cartesian coordinate in y direction
Ψ stream function
*θ* temperature
Dimensionless numbers
*Ec* Eckert number
*Gr* Grashof number
*Ha* Hartmann number
*Nu* Nusselt number
*Pr* Prandtl number
*Ra* Rayleigh number
*Re* Reynolds number

## REFERENCES


[1] Oreper GM, Szekely J. The effect of an externally imposed magnetic field on buoyancy driven flow in a rectangular cavity. J. Cryst. Growth 1983; 64: 505-15. https://doi.org/10.1016/0022-0248(83)90335-4.

[2] Mohamad AA, Viskanta R. Transient low Prandtl number fluid convection in a lid-driven cavity. Numer. Heat Transf. A 1991; 19: 187-205. https:// doi.org/10.1080/10407789108944845

[3] Garandet JP, Alboussiere JP, Moreau T. Buoyancy driven convection in a rectangular cavity with a transverse magnetic field. Int. J. Heat Mass Transf. 1992; 35: 741-48. https://doi.org/10.1016/0017-9310(92)90242-K

[4] Rudraiah N, Barron RM, Venkatachalappa M, Subbaraya CK. Effect of a magnetic field on free convection in a rectangular enclosure. Int. J. Eng. Sci. 1995; 33: 1075-84. https://doi.org/10.1016/0020-7225(94)00120-9

[5] Al-Najem NM, Khanafer KM, El-Refaee MM. Numerical study of laminar natural convection in tilted enclosure with transverse magnetic field. Int J Numer Method H 1998; 8: 651–72. https://doi.org/10.1108/09615539810226094

[6] Sarris IE, Kakarantzas SC, Grecos AP, Vlachos NS. MHD natural convection in a laterally and volumetrically heated square cavity. Int. J. Heat Mass Transf. 2005; 48: 3443–53. https://doi.org/10.1016/j.ijheatmasstransfer.2005.03.014

[7] Kandaswamy P, MalligaSundari S, Nithyadevi N. Magnetoconvection in an enclosure with partially active vertical walls. Int. J. Heat Mass Transf. 2008; 51: 1946–54. https://doi.org/10.1016/j.ijheatmasstransfer.2007.06.025

[8] Borghi CA, Cristofolini A, Minak G. Numerical methods for the solution of the electrodynamics in magnetohydrodynamic flows. IEEE T Magn 1996; 32: 1010-13. https://doi.org/10.1109/20.497411

[9] Borghi CA, Carraro MR, Cristofolini A. Numerical solution of the nonlinear electrodynamics in MHD regimes with magnetic Reynolds number near one. IEEE T Magn 2004; 40: 593-6. https://doi.org/10.1109/TMAG.2004.825414

[10] Verardi SLL., Cardoso JR. A solution of two-dimensional magneto−hydrodynamic flow using the finite element method. IEEE T Magn 1998; 34: 3134-7. https://doi.org/10.1109/20.717734

[11] Verardi SLL, Cardoso JR, Costa MC. Three-dimensional finite element analysis of MHD duct flow by the penalty function formulation. IEEE T Magn 2001; 37: 3384-7. https://doi.org/10.1109/20.952619

[12] Verardi SLL, Machado JM, Cardoso JR. The element-free Galerkin method applied to the study of fully developed magneto−hydrodynamic duct flows. IEEE T Magn 2002; 38: 941-4. https://doi.org/ 10.1109/20.996242

[13] Shadid JN, Pawlowski RP, Banks JW, Chacon L, Lin PT, Tuminaro RS. Towards a scalable fully-implicit fully-coupled resistive MHD formulation with stabilized FE methods. J. Comput. Phys. 2010; 229: 7649–71. https://doi.org/10.1016/j.jcp.2010.06.018

[14] Taghikhani MA. Magnetic field effect on natural convection flow with internal heat generation using fast Ψ – Ω method. J Appl Fluid Mech 2015; 8: 189-96. https://doi.org/10.18869/acadpub.jafm.67.221.19377

[15] Taghikhani MA. Numerical study of magneto-convection inside an enclosure using enhanced stream function-vorticity formulation. Sci Iran B 2015; 22: 854-64. https://doi.org/ 10.1109/TMAG.2009.2018959

[16] Ece MC, Buyuk E. Natural convection flow under magnetic field in an inclined rectangular enclosure heated and cooled on adjacent walls. Fluid Dyn. Res. 2006; 38: 564-90. https://doi.org/10.1016/j.fluiddyn.2006.04.002

[17] Ece MC, Büyük E. Natural convection flow under a magnetic field in an inclined square enclosure differentially heated on adjacent walls. Meccanica 2007; 42: 435–49. https://doi.org/ 10.1007/s11012-007-9067-5

[18] Rashidi MM, Nasiri M, Khezerloo M, Laraqi N. Numerical investigation of magnetic field effect on mixed convection heat transfer of nanofluid in a channel with sinusoidal walls. J. Magn. Magn. Mater. 2016; 401:159–68. https://doi.org/10.1016/j.jmmm.2015.10.034

[19] Bourantas GC, Loukopoulos VC. MHD natural-convection flow in an inclined square enclosure filled with a micropolar-nanofluid. Int. J. Heat Mass Transf. 2014; 79: 930–44. https://doi.org/10.1016/j.ijheatmasstransfer.2014.08.075

[20] Heidary H, Hosseini R, Pirmohammadi M, Kermani MJ. Numerical study of magnetic field effect on nano-fluid forced convection in a channel. J. Magn. Magn. Mater. 2015; 374: 11–17. https://doi.org/10.1016/j.jmmm.2014.08.001

[21] Sheikholeslami M, Hayat T, Alsaedi A. Numerical study for external magnetic source influence on water based nanofluid convective heat transfer. Int. J. Heat Mass Transf. 2017; 106: 745–55. https://doi.org/10.1016/j.ijheatmasstransfer.2016.09.077

[22] Sheikholeslami M, Ganji DD. Ferrohydrodynamic and magnetohydrodynamic effects on ferrofluid flow and convective heat transfer. Energy 2014; 75: 400-10. https://doi.org/10.1016/j.energy.2014.07.089

[23] Sheikholeslami M, GorjiBandpy M, Ellahi R, Zeeshan A. Simulation of MHD CuO-water nanofluid flow and convective heat transfer considering Lorentz forces. J. Magn. Magn. Mater. 2014; 369: 69–80. https://doi.org/10.1016/j.jmmm.2014.06.017

[24] Selimefendigil F, Oztop HF. Analysis of MHD mixed convection in a flexible walled and nanofluids filled lid-driven cavity with volumetric heat generation. Int. J. Mech. Sci. 2016; 118: 113–24. https://doi.org/10.1016/j.ijmecsci.2016.09.011

[25] Selimefendigil F, Oztop HF. Mixed convection in a partially heated triangular cavity filled with nanofluid having a partially flexible wall and internal heat generation. J Taiwan Int Chem E 2017; 70: 168–78. https://doi.org/10.1016/j.jtice.2016.10.038

[26] Selimefendigil F, Oztop HF. Natural convection in a flexible sided triangular cavity with internal heat generation under the effect of inclined magnetic field. J. Magn. Magn. Mater. 2016; 417: 327–37. https://doi.org/10.1016/j.jmmm.2016.05.053

[27] Selimefendigil F, Oztop HF. Mixed convection of nanofluid filled cavity with oscillating lid under the influence of an inclined magnetic field. J Taiwan Int Chem E 2016; 63: 202–15. https://doi.org/10.1016/j.jtice.2016.03.003

[28] Selimefendigil F, Oztop HF, Chamkha AJ. MHD mixed convection and entropy generation of nanofluid filled lid driven cavity under the influence of inclined magnetic fields imposed to its upper and lower diagonal triangular domains. J. Magn. Magn. Mater. 2016; 406: 266–81. https://doi.org/10.1016/j.jmmm.2016.01.039

[29] Sheremet MA, Oztop HF, Pop I. MHD natural convection in an inclined wavy cavity with corner heater filled with a nanofluid. J. Magn. Magn. Mater. 2016; 416: 37–47. https://doi.org/10.1016/j.jmmm.2016.04.061

[30] Ghaffarpasand O. Numerical Study of MHD Natural Convection Inside a Sinusoidally Heated Lid-Driven Cavity Filled with Fe3O4-water Nanofluid in the Presence of Joule Heating. Appl. Math. Model. 2016; 40: 9165–82. https://doi.org/10.1016/j.apm.2016.05.038

[31] Hussain S, Ahmad S, Mehmood K, Sagheer M. Effects of inclination angle on mixed convective nanofluid flow in a double lid-driven cavity with discrete heat sources. Int. J. Heat Mass Transf. 2017; 106: 847–60. https://doi.org/10.1016/j.ijheatmasstransfer.2016.10.016

[32] Hussain S, Mehmood K, Sagheer M. MHD mixed convection and entropy generation of water-alumina nanofluid flow in a double lid driven cavity with discrete heating. J. Magn. Magn. Mater. 2016; 419: 140–55. https://doi.org/10.1016/j.jmmm.2016.06.006

[33] Job VM, Gunakala SR. Mixed convection nanofluid flows through a grooved channel with internal heat generating solid cylinders in the presence of an applied magnetic field. Int. J. Heat Mass Transf. 2017;107: 133–45. https://doi.org/10.1016/j.ijheatmasstransfer.2016.11.021

[34] Karimipour A, Taghipour A, Malvandi A. Developing the laminar MHD forced convection flow of water/FMWNT carbon nanotubes in a microchannel imposed the uniform heat flux. J. Magn. Magn. Mater. 2016; 419: 420–28. https://doi.org/10.1016/j.jmmm.2016.06.063

[35] Ismael MA, Mansour MA, Chamkha AJ, Rashad AM. Mixed convection in a nanofluid filled-cavity with partial slip subjected to constant heat flux and inclined magnetic field. J. Magn. Magn. Mater. 2016; 416: 25–36. https://doi.org/10.1016/j.jmmm.2016.05.006

[36] Aghaei A, Khorasanizadeh H, Sheikhzadeh GA, Abbaszadeh M. Numerical study of magnetic field on mixed convection and entropy generation of nanofluid in a trapezoidal enclosure. J. Magn. Magn. Mater. 2016; 403: 133–45. https://doi.org/10.1016/j.jmmm.2015.11.067

[37] Mehrez Z, El Cafsi A, Belghith A, Le Quéré P. MHD effects on heat transfer and entropygeneration of nanofluid flow in an open cavity. J. Magn. Magn. Mater. 2015; 374: 214–24. https://doi.org/10.1016/j.jmmm.2014.08.010

[38] Chamkha AJ, Ismael M, Kasaeipoor A, Armaghani T. Entropy generation and natural convection of CuO-water nanofluid in C-shaped cavity under magnetic field. Entropy 2016; 18: 1-18. https://doi.org/10.3390/e18020050

[39] Chamkha AJ, Rashad AM, Mansour MA, Armaghani T, Ghalambaz M. Effects of heat sink and source and entropy generation on MHD mixed convection of a Cu-water nanofluid in a lid-driven square porous enclosure with partial slip. Phys. Fluids 2017; 29: 052001. https://doi.org/10.1063/1.4981911

[40] Rashad AM, Armaghani T, Chamkha AJ, Mansour MA. Entropy generation and MHD natural convection of a nanofluid in an inclined square porous cavity: Effects of a heat sink and source size and location. Chin. J. Phys. 2018; 56: 193-211. https://doi.org/10.1016/j.cjph.2017.11.026

[41] Chamkha AJ, Rashad AM, Armaghani T, Mansour MA. Effects of partial slip on entropy generation and MHD combined convection in a lid-driven porous enclosure saturated with a Cu–water nanofluid. J. Therm. Anal. Calorim. 2018; 132: 1291-306. https://doi.org/10.1007/s10973-017-6918-8

[42] Armaghani T, Esmaeili H, Mohammadpoor YA, Pop I. MHD mixed convection flow and heat transfer in an open C-shaped enclosure using water-copper oxide nanofluid. Heat Mass Transfer 2018; 54: 1791-801. https://doi.org/10.1007/s00231-017-2265-3

[43] Abedini A, Armaghani T, Chamkha AJ. MHD free convection heat transfer of a water–$Fe_3O_4$nanofluid in a baffled C-shaped enclosure. J. Therm. Anal. Calorim., https://doi.org/10.1007/s10973-018-7225-8.

[44] Koo J, Kleinstreuer C. Laminar nanofluid flow in microheat-sinks. Int. J. Heat Mass Transf. 2005; 48: 2652–61. https://doi.org/10.1016/j.ijheatmasstransfer.2005.01.029

[45] Tian ZF, Yu PX. An efficient compact difference scheme for solving the streamfunction formulation of the incompressible Navier−Stokes equations. J. Comput. Phys. 2011; 230: 6404−19. https://doi.org/10.1016/j.jcp.2010.12.031

[46] Dixit HN, Babu V. Simulation of high Rayleigh number natural convection in a square cavity using the lattice Boltzmann method. Int. J. Heat Mass Transf. 2006; 49: 727-39. https://doi.org/10.1016/j.ijheatmasstransfer.2005.07.046

[47] Kuznik F, Vareilles J, Rusaouen G, Krauss G. A double-population lattice Boltzmann method with non-uniform mesh for the simulation of natural convection in a square cavity. Int J Heat Fluid Fl 2007; 28: 862–70. https://doi.org/10.1016/j.ijheatfluidflow.2006.10.002

[48] Moumni H, Welhezi H, Djebali R, Sediki E. Accurate finite volume investigation of nanofluid mixed convection in two sided lid driven cavity including discrete heat sources. Appl. Math. Model. 2015; 39: 4164-79. https://doi.org/10.1016/j.apm.2014.12.035

[49] Djebali R, El Ganaoui M, Sammouda H, Bennacer R. Some benchmarks of a side wall heated cavity using lattice Boltzmann approach. Fluid Dyn. Mater. Process. 2009; 5: 261-82. https://doi.org/10.3970/fdmp.2009.005.261

[50] Tian Z, Ge Y. A fourth-order compact finite difference scheme for the steady stream function–vorticity formulation of the Navier–Stokes/Boussinesq equations. Int J Numer Meth Fl 2003; 41: 495–518. https://doi.org/10.1002/fld.444

[51] Nonino C, Croce G. An equal-order velocity-pressure algorithm for incompressible thermal flows, part 2: validation. Numer. Heat Transf. B 1997; 32: 17-35. https://doi.org /10.1080/10407799708914997

[52] Kalita JC, Dalal DC, Dass AK. Fully compact higher-order computation of steady-state natural convection in a square cavity. Phys Rev E 2001; 64: 066703. https://doi.org/10.1103/PhysRevE.64.066703

[53] Arpino F, Massarotti N, Mauro A. High Rayleigh number laminar-free convection in cavities: new benchmark solutions. Numer. Heat Transf. B 2010; 58: 73-97. https://doi.org/10.1080/10407790.2010.508438
[54] Sarris IE, Zikos GK, Grecos AP, Vlachos NS. On the limits of validity of the low magnetic Reynolds number approximation in MHD natural-convection heat transfer. Numer. Heat Transf. B 2006; 50: 157–80. https://doi.org/10.1080/10407790500459403
[55] Pirmohammadi M, Ghassemi M. Effect of magnetic field on convection heat transfer inside a tilted square enclosure. Int Commun Heat Mass 2009; 36: 776–80. https://doi.org/10.1016/j.icheatmasstransfer.2009.03.023
[56] Piazza ID, Ciofalo M. MHD free convection in a liquid-metal filled cubic enclosure. II. internal heating. Int. J. Heat Mass Transf. 2002; 45: 1493–511. https://doi.org/10.1016/S0017-9310(01)00253-8